# Effect of electric field on carrier escape mechanisms in quantum dot intermediate band solar cells

Yushuai Dai (戴宇帅),[1] Stephen J. Polly,[1] Staffan Hellstroem,[1,a)] Michael A. Slocum,[1] Zachary S. Bittner,[1] David V. Forbes,[1] Paul J. Roland,[2] Randy J. Ellingson,[2] and Seth M. Hubbard[1,b)]
[1]*Nanopower Research Laboratories, Rochester Institute of Technology, Rochester, New York 14623, USA*
[2]*Wright Center for Photovoltaic Innovation and Commercialization (PVIC), The University of Toledo, Toledo, Ohio 43606, USA*

(Received 26 September 2016; accepted 9 December 2016; published online 3 January 2017)

Carrier escape and recombination from quantum dot (QD) states reduce the probability of two-step photon absorption (TSPA) by decreasing the available carrier population in the intermediate band (IB). In order to optimize the second photon absorption for future designs of quantum dot embedded intermediate band solar cells, the presented study combined the results of simulations and experiments to quantify the effect of electric field on the barrier height and the carrier escape from the QDs in InAs/GaAs quantum dot solar cells with five-layer QD superlattices. The electric field dependent effective barrier heights for ground state electrons were calculated using eight band $k{\cdot}p$ theory at short circuit conditions. With an increase in electric field surrounding the QDs from 5 kV/cm to 50 kV/cm, the effective barrier height of the ground state electrons was reduced from 147 meV to 136 meV, respectively. Thus, the increasing electric field not only exponentially enhances the ground state electron tunneling rate (effectively zero at 5 kV/cm and $7.9 \times 10^6\,s^{-1}$ at 50 kV/cm) but also doubles the thermal escape rate ($2.2 \times 10^{11}\,s^{-1}$ at 5 kV/cm and $4.1 \times 10^{11}\,s^{-1}$ at 50 kV/cm). Temperature-dependent external quantum efficiency measurements were performed to verify that the increasing electric field decreases the effective barrier height. Additionally, the electric field dependent radiative lifetimes of the ground state were characterized with time-resolved photoluminescence experiments. This study showed that the increasing electric field extended the radiative recombination lifetime in the ground state of the QDs as a consequence of the reduced wave-function overlap between the electrons and holes. The balance of carrier escape and recombination determines the probability of TSPA. *Published by AIP Publishing.*
[http://dx.doi.org/10.1063/1.4972958]

## I. INTRODUCTION

The concept of intermediate band solar cells (IBSC)[1,2] has been proposed as a method of achieving a conversion efficiency of 63% with maximum concentrated light illumination using detailed balance calculations. Between the conduction band (CB) and the valence band (VB), the ideal intermediate band IB is a band that is partially filled with electron in quasi-thermal equilibrium to support sequential optical absorption.[3] The IBSC enables two-step photon absorption (TSPA), first an optical transition from the VB to the IB followed by an optical transition from the IB to the CB, so the IBSC increases output current by extending the absorption to sub-band-gap photons. Consequently, the IBSC operates as three current sources: two in series (VB-IB transition and IB-CB transition) are in parallel with the original bulk diode (VB-CB transition). This allows the IBSC to maintain the voltage output of bulk host material. So far, quantum dots (QDs) have been considered as one of few materials systems to form an IB for the realization of IBSC concepts.[3] The confined levels of QDs can be tuned by varying QD size, or through selection of QD or barrier material. A zero density of states between the confined states of electrons reduces the thermal coupling, helping to facilitate the two-photon-absorption process. Due to mature growth techniques in metalorganic vapor phase epitaxy (MOVPE) and molecular beam epitaxy (MBE), GaAs solar cells with embedded InAs-GaAs quantum dots (QDs) in the intrinsic region have been widely studied.[4–7]

Many studies have shown enhanced sub-band-gap carrier collection in InAs/GaAs quantum dot solar cells (QDSCs).[6–8] However, if the increase in current from the VB to IB transition occurs by either thermal escape or tunneling, the open-circuit voltage of the host material is sacrificed because of coupling between the IB and CB. To maintain the voltage of the bulk material (also known as a voltage preservation), the IB should be completely separated from the CB and the second photon absorption (transition from the IB to CB) should be the dominant process of the carriers in the IB.[6] To enable quasi-Fermi level splitting between IB and CB, thermal escape should be suppressed. Therefore, although experimental observation of the second photon absorption has been observed at both low temperature[9–11] and room temperature,[12–14] the voltage preservation so far has only been shown at low temperature.[15,16] To increase the

a)Now at Finisar Corporation.
b)Author to whom correspondence should be addressed. Electronic mail: smhsps@rit.edu.

sub-band-gap carrier collection via the second photon absorption, other competing processes, including thermal escape, tunneling, and recombination, must be reduced.

Because the QDs are usually embedded in the intrinsic regions of the diode, they exist within an electric field formed by the built-in potential that is then affected by external bias. It is important, therefore, to investigate the effect of electric field on carrier escape and radiative recombination. Many published studies have investigated the effect of electric field on the QD-IBSC. Antolin *et al.* demonstrated that an electric field (>100 kV/cm) enhanced tunneling escape of carriers and demonstrated suppressed tunneling through application of a thick GaAs spacer layer between QDs in InAs/GaAs QDSCs.[6] Because the thick spacer layer limited the number of QD that could be grown in the intrinsic region, Ramiro *et al.* further improved the spacer layer design by inserting a field damping layer to reduce the electric field and observed that voltage preservation can be achieved even if tunneling exists at short circuit conditions.[16] Elborg *et al.* experimentally revealed that a maximum in TSPA occurred at a reverse bias of −0.3 V in GaAs/AlGaAs QDSCs.[17] Creti *et al.* demonstrated that the effect of electric field on electron-hole separation along the growth direction can be used to preserve TSPA up to room temperature.[10] Kasamatsu *et al.* has shown that a strong internal electric field of 193 kV/cm severely reduces the radiative lifetime of the ground state (GS) carriers thereby quenching TSPA, but internal electric fields on the order of 10 kV/cm still maintain QD electronic coupling.[18] Obviously, the electric field significantly affects TSPA efficiency and the performances of QD-IBSCs. However, the effect of electric field on the other more dominant mechanisms of carrier escape and recombination has not yet been fully understood and published, especially with regard to the barrier height and the radiative lifetime. In this work, quantitative analysis of the effect of electric field on thermal escape and tunneling escape in five-layer QDSC structures is presented. The simulations of the QD band structures using the eight-band $k\cdot p$ theory is corroborated with temperature dependent external quantum efficiency (TDEQE) measurements to characterize carrier escape from the QDs. Time-resolved photoluminescence (TRPL) experiments were also applied to detect the electric field dependent radiative recombination dynamics.

## II. SAMPLE AND EXPERIMENT

Three QD embedded *p-i-n* GaAs solar cell samples with a varied local electric field around the QDs were prepared and studied. The structures were grown on a 350 $\mu$m thick Si-doped GaAs (100) substrate misoriented 2° toward to the [110] direction, using a low-pressure rotating disk metal organic vapor phase epitaxy (MOVPE) reactor (Veeco D125LDM).[19] As shown in Figure 1, three separate devices with a five-layer superlattice of QDs were grown in the 600 nm (unintentionally n-type doped $1\times10^{16}\,\mathrm{cm}^{-3}$) intrinsic region of a pin GaAs solar cell, each with QDs in different locations: emitter shifted (33 nm from the p-emitter), at the center or near the base (33 nm from the n-base). The QD super-lattice consisted of 1.8 ML of InAs deposited at

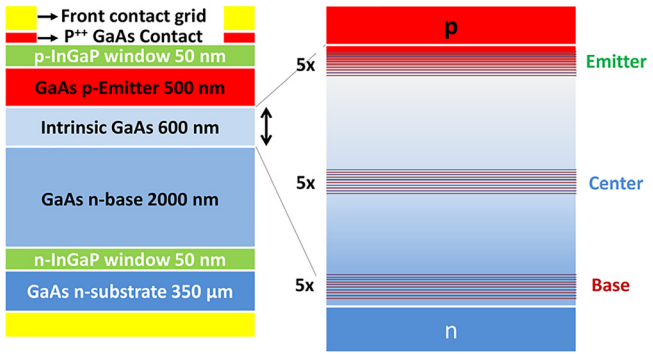


FIG. 1. Schematic drawing of structural layer layout for QD embedded GaAs p-i-n solar cell devices.

500 °C. After growth of a low temperature GaAs capping layer, temperature was then ramped to 585 °C for the growth of the GaAs spacer layers and a thin (1.1–1.4 nm) GaP strain compensation layer. The average size of hemisphere-shaped QDs, measured via atomic force microscopy (AFM), is 2–5 nm in height and 15–25 nm in diameter.[20] Thin (50 nm) InGaP front and back window layers were employed to reduce surface and interface recombination. The base consisted of 2000 nm of Si-doped GaAs with a dopant density of $1\times10^{17}\,\mathrm{cm}^{-3}$ while the emitter consisted of 500 nm of Zn-doped GaAs with a dopant density of $2\times10^{18}\,\mathrm{cm}^{-3}$. Finally, a heavily doped GaAs contact layer was used for ohmic contact formation. Solar cells were then fabricated using standard III–V processing and microlithography techniques. Individual cells were isolated using wet chemical etching and the contact layer was selectively wet etched to the front InGaP window after the metallization to eliminate parasitic absorption effects. Anti-reflective coatings were not used. Measurements were performed on $1\times1\,\mathrm{cm}^2$ grid-finger free quantum efficiency pad.

Room temperature External Quantum Efficiency (EQE) measurements were taken with a Newport IQE-200 Spectroradiometric Measurement system using Standford Research SR570 preamplifier and SR830 lock-in amplifier. Temperature dependent EQE measurements were analyzed using an OL750 Spectroradiometric Measurement system in a CryoIndustries 10 K M-22 cryo-system. TRPL was measured by a Becker & Hickel single photon counting module (SPC-130-E/M) and a Hamamatsu near infrared photomultiplier tube (H10330a-45), with a temporal resolution of 20 ps. TRPL excitation wavelength was provided by a Fianium supercontinuum white laser source (SC400-2) with an Acusto-Optical Tuning Filter set to 800 nm with a repetition rate of 10 MHz (flux of $8.8\times10^{11}$ photon/cm$^2$·s). TRPL measurements were held at 15 K by an Advanced Research System 10 K DE-202 closed loop helium cryostat.

## III. RESULTS AND DISCUSSION

### A. Simulation

Because of non-negligible n-type background doping ($1\times10^{16}\,\mathrm{cm}^{-3}$) in the 600 nm unintentionally doped (uid) "intrinsic" region of the *p-i-n* diodes, the electric field is maximized near the p-type emitter and decreases towards the

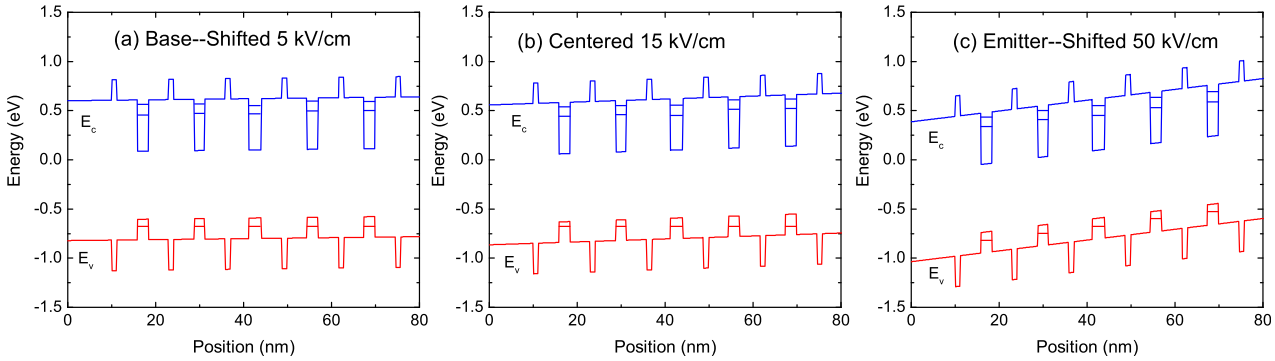


FIG. 2. Calculated band structure of different QD local electric field under short circuit conditions: (a) The base-shifted QDs with local electric field of 5 kV/cm, (b) the centered QDs with local electric field of 15 kV/cm, and (c) the emitter-shifted QDs with local electric field of 50 kV/cm.

position close to the n-type base. The details of simulation of the electric field can be found in a previous publication.[4] Therefore, the electric field around the QDs varies with the depth across the intrinsic region under short circuit conditions. In order to theoretically investigate the effect of electric field in the QDSCs within the three designs, the band structures of InAs/GaAs quantum dots embedded in the intrinsic region of a pin solar cell were simulated using a finite-difference discretization method of the eight-band $\boldsymbol{k}\cdot\boldsymbol{p}$ Hamiltonian.[21] A Poisson-Schrodinger solver was written in C++ program with material parameters from the most cited literature.[22] The temperature was set at 300 K. Based on the AFM results shown in prior work,[20] the average height, radius, and the wetting layer (WL) thickness of a single hemispherical quantum dot were set at 3 nm, 10 nm, and 0.5 nm, respectively. In addition, 1.3 nm GaP as a strain compensation layer was inserted between the dots, so the total dot-dot distance was set at 14 nm.

Figures 2(a), 2(b), and 2(c) show the simulated band structures at 300 K under open circuit conditions of the five-layer-QD super-lattice with local electric field of 5 kV/cm (base-shifted, 33 nm from the n-base), 15 kV/cm (centered), and 50 kV/cm (emitter-shifted, 33 nm from the p-emitter), respectively. Due to the increasing local electric field around the QDs, the band bending experienced by the QDs at the three positions is illustrated. The blue line refers to the conduction band. Two localized energy levels of electrons are shown in each QD. The energy difference between each of the localized energy levels and the edge of the conduction band is referred to as the barrier height of the electron. The red line represents the valence band and the ground state of holes. Due to the multiple states (heavy, light, and split off) of the holes, there are too many excited states (ESs) to be shown.

Figure 3(a) shows the extracted average electron barrier heights. Because the electric field acts as another perturbation to the Hamiltonian that changes the wave-functions of the electrons, the electric field lowers the confined level of the electrons and extends the conduction band edge. The barrier height of both ground state and excited state electrons decreases slightly with increasing electric field. At a local electric field of 5 kV/cm, the barrier height of the electron ground state and the excited state is 147 meV and 68 meV, respectively. Increasing QD local electric field to 15 kV/cm decreases the barrier height to 141 meV from the ground state and 64 eV from the excited state. When the local electric field is 50 kV/cm, the barrier height of the electron from the ground state and excited state is 136 meV and 60 meV, respectively. Similar to the electrons barrier heights, the average barrier height of the ground state holes is 137 meV, 130 meV, and 117 meV for the increasing electric field of 5 kV/cm, 15 kV/cm, and 50 kV/cm, respectively. Due to shifting of the confined levels of electrons and holes under an electric field, the state becomes affected by the quantum confined stark effect (QCSE).[23] Using the subtraction between the band-edge of the GaAs and the barrier height of the ground state electron and hole, the calculated transition energy between the ground state electron and holes (H1-E1) red shifts from 1.13 eV (1097 nm) under the electric field of 5 kV/cm to 1.12 eV (1107 nm) under the electric field of

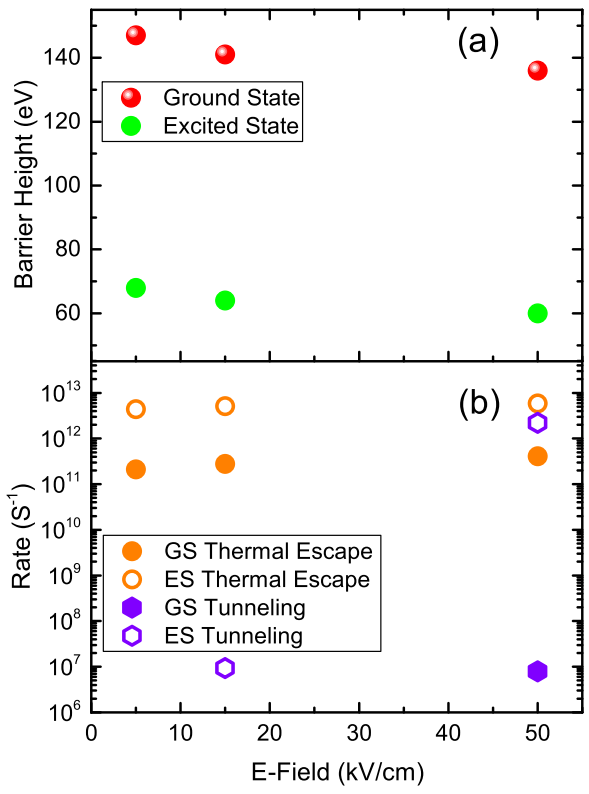


FIG. 3. Parameters extracted from the band structure simulation at 300 K: (a) average barrier height; (b) thermal escape rate and tunneling rate.

50 kV/cm at 300 K. However, because of the limited absorption from the five layer ground state QD,[24] carrier collection from photon energies below 1.1 eV (>1100 nm) is negligible.

Using the extracted barrier height, the thermal escape rate from different energy levels can be estimated using Equation (1).[25] Due to the small height to diameter aspect ratio, quantum confinement is mainly along the QD layer growth axis, which is similar to a quantum well structure. For simplification, the thermal escape rate exponentially decreases with the ratio of field dependent barrier height and temperature as shown in the following equation:

$$\frac{1}{\tau_{\mathrm{th}}} = \frac{1}{\mathrm{L_z}}\sqrt{\frac{\mathrm{kT}}{2\pi \mathrm{m_Q}}}\exp\left(-\frac{\mathrm{E_b}}{\mathrm{kT}}\right). \tag{1}$$

Here, $m_Q$ is the carrier's effective mass in the quantum confinement, $L_z$ is the height of the QDs (3 nm), $E_b$ is the barrier height, $k$ is Boltzmann's constant, and $T$ is temperature. Equation (2) is the inverse of tunneling probability per unit time. The tunneling probability was originally estimated using transfer matrix technique in the effective mass approximation.[26] In order to highlight the basic physical trends in the tunneling rate, Equation (2) is simplified by assuming transmission through a single barrier[27,28]

$$\frac{1}{\tau_{tun}} = \frac{1}{L_z^2}\frac{n\pi\hbar}{2m_Q}\exp\left(-\frac{2}{\hbar}\int_0^b \sqrt{2m_b(E_b - qFz)}dz\right). \tag{2}$$

Here, $\hbar$ is Planck's constant, $b$ is the thickness of the barrier, $F$ is the strength of the electric field, and $m_b$ is the carrier effective mass in the barrier. By assuming an electron mass in InAs of $0.023m_0$ and in GaAs of $0.063m_0$,[29] Figure 2(b) shows the calculated thermal escape rate ($1/\tau_{th}$) and tunneling rate ($1/\tau_{tun}$) of electrons for different confined energy levels. First, regardless of electric field at 300 K, thermal escape dominates electron escape from the ground state, with a rate on the order of $10^{11}\,\mathrm{s}^{-1}$. For ground state electrons, the tunneling rate is too slow ($<10^{-12}\,\mathrm{s}^{-1}$) to show in Figure 3(b) under low electric field conditions ($\leq$15 kV/cm). The ground state tunneling rate increases near $10^7\,\mathrm{s}^{-1}$ at 50 kV/cm. For the electrons in the excited states, thermal escape dominates in the QDSCs with lower electric field around the QDs (5 kV/cm and 15 kV/cm). However, when the electric field around the QD layer reaches 50 kV/cm, the tunneling rate ($2\times10^{12}\,\mathrm{s}^{-1}$) is comparable with the thermal escape rate ($6\times10^{12}\,\mathrm{s}^{-1}$). Second, increasing electric field around QDs decreases the effective barrier height, so the increased local electric field enhances both tunneling and thermal escape, albeit with a much more obvious effect on tunneling. The tunneling rate increases exponentially with increasing electric field magnitude according to Equation (2).

The dynamics of the ground state electron also need to be considered when evaluating the physics of the IBSC. Along with carrier escape (tunneling and thermal escape), there are three other processes that happen to electrons in the ground state of QDs, including non-radiative recombination, radiative recombination, and TSPA. The lifetime ($\tau_{total}$) of the ground state carriers consists of the five rate components shown in the following equation:

$$\frac{1}{\tau_{\mathrm{total}}} = \frac{1}{\tau_{nr}} + \frac{1}{\tau_r} + \frac{1}{\tau_{th}} + \frac{1}{\tau_{tun}} + \frac{1}{\tau_{TSPA}}. \tag{3}$$

Here, $\tau_{nr}$ is the non-radiative recombination component which is usually negligible inside high quality QDs because few defects are formed during volumetric strain relaxation.[30,31] $\tau_r$ is the radiative recombination lifetime which depends on wave-function overlap[32] and carrier distribution.[33] The typical values of $\tau_r$ from the ground state carrier in InAs/GaAs QD is usually between 0.5 and 5 ns, depending on the size and the number of repeat layers of QDs.[34–36] The optical generation rate from the ground state to the conduction band, $1/\tau_{TSPA}$, depends on the product of incident photon flux and optical capture cross section,[37,38] and has been shown to be on the order of $1\times10^8\,\mathrm{s}^{-1}$ under $1\times10^4$ sun concentration.[39] Thus, for the InAs/GaAs QD-IBSC at 300 K, although the ground state tunneling rate reaches $8\times10^6\,\mathrm{s}^{-1}$ at 50 kV/cm, the thermal escape ($10^{11}\,\mathrm{s}^{-1}$) will limit TSPA under concentrated illumination. In order to enable TSPA to be dominant at room temperature, barrier modifications with wide band gap material including InGaP[40,41] or AlGaAs[42,43] are being considered for the IBSC design to suppress the thermal coupling between the IB and CB at the room temperature. The radiative recombination ($10^8$–$10^9\,\mathrm{s}^{-1}$) also reduces the efficiency of TSPA in InAs/GaAs QD. Because the radiative recombination is the inverse process of optical absorption, to increase TSPA by increasing ground state radiative recombination lifetime, the QD-IBSC design should optimize the trade-off between absorption and recombination. Photon recycling[44] is one option that could be considered to relieve loss due to radiative recombination.

### B. Experiment

In order to experimentally assess the electric field dependent carrier escape from QD absorption (VB-IB), Figure 4(a) shows the 300 K EQE in semi-log scale of the three investigated QDSCs. There are five peaks in total, including EQE from the wetting layer (WL, around 910 nm), three transitions between excited states of holes and the excited state electrons (ES, 920 nm–1020 nm), and the ground state (GS, around 1060 nm). The ground state refers the transition from excited states of holes to the ground state of the electrons. The ground state transition (H1 to E1) above 1100 nm is too weak to detect from the five-layer-QD absorption as mentioned in the simulation section. With increasing local electric field intensity of the QDs from 5 kV/cm to 50 kV/cm, the overall sub-GaAs band-gap EQE increases. The integrated sub-band-gap AM0 short circuit current ($J_{sc}$ for $\lambda > 880$ nm) is 108 $\mu$A/cm$^2$, 117 $\mu$A/cm$^2$, and 119 $\mu$A/cm$^2$ for the QDSC with 5 kV/cm, 15 kV/cm, and 50 kV/cm, respectively. The electric field enhanced sub-band-gap carrier collection is caused by the increased rate of the tunneling and thermal escape, which correlates with the calculations in Figure 3(b). The absorption edge is red shifted with the increasing electric field around the QDs, which is due the QCSE.

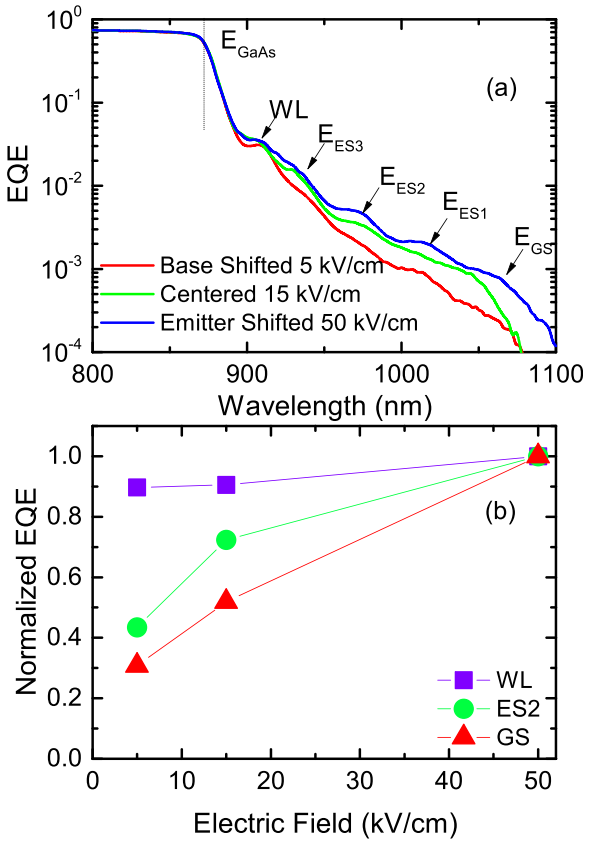


FIG. 4. 300K EQE of the three investigated cell under zero external bias. (b) Electric field dependent sub-band-gap EQE normalized to 50 kV/cm.

Figure 4(b) shows the electric field dependent sub-band-gap EQE normalized to 50 kV/cm. The carrier collection from the WL shows a slight increase with increasing electric field, which indicates that almost all carriers can be collected from the wetting layer at 300 K even at 5 kV/cm. The increase is because even though the thermal escape dominates the shallow WL levels, higher electric fields may provide a slight increase in escape due to both barrier lowering and carrier tunneling. When the electric field increases from 5 kV/cm to 50 kV/cm, the carrier collection from ES2 increased 60%, while the carrier collection from GS increased 70%. Based on the low tunneling rates calculated in Figure 3(b), this large increase was not expected except perhaps in either ES at fields over 50 kV/cm. There may be three possible reasons for this: (1) The QCSE separates the electron and hole wavefunction, which causes a red shifted[45] and broadened[46] sub-bandgap absorption spectra. Fry *et al.* found that an increasing tail of GaAs (Franz-Keldysh effects) and wetting layer photocurrent affects the QD region with greater reverse bias in a single layer InAs/GaAs QD pin structure.[47] Therefore, the enhanced ground state carrier collection with increasing electric field may be due to the electric field introduced boarding of the optical transitions between higher energy states. (2) After carriers escape from QD, the carriers may be recaptured and recombine in the wetting layer and QDs.[48] Increased electric field improves the charge separation[10] and reduces the number of carriers within the QD region, so the carrier collection increases with increasing electric field. (3) Although the QCSE reduces the absorption rate in the QD ground state[46] due to spatial separation of electron and hole wave-function, the associated increasing radiative recombination lifetime of the ground state carriers may contribute to enhanced carrier collection.

The room temperature sub-GaAs-bandgap EQE experimentally verifies the electric field enhanced carrier escape rate in InAs/GaAs QDSC. The electric field enhanced carrier escape limits TSPA and associated IBSC applications. However, the radiative recombination process may also affect TSPA from Equation (3). To experimentally detect the effect of electric field on the radiative lifetime of the ground state, TRPL measurements were conducted. The TRPL spectra represent the decay rates of PL from the QD ground state. The decay time depends on the total lifetime. Carrier dynamics of the ground state electron can be given as[49]

$$\frac{d(N(t))}{dt} = -\frac{N(t)}{\tau_{total}}. \tag{4}$$

Here, $N(t)$ is the total number of carriers in the QD ground state. In order to isolate the radiative recombination lifetime, the other components should be evaluated. The earlier simulations shows the electron thermal escape is the fastest ($10^{11}\,s^{-1}$) at 300 K for all samples, so the thermal escape components should be suppressed by lowering temperature. The very slow ground state electron tunneling rate (less than $10^{-12}\,s^{-1}$) with 5 kV/cm and 15 kV/cm electric field strengths cannot change the TRPL signal. The 50 kV/cm electric field increases the ground state electron tunneling rate towards $10^{7}\,s^{-1}$, but radiative recombination ($10^{8}\,s^{-1}$ to $10^{9}\,s^{-1}$) is the dominant process, so the time component extracted at low temperature (15 K) refers to the radiative recombination lifetime.

Figure 5 shows the electric field dependent ground state TRPL at 15 K. The QDSCs with 5 kV/cm field show a mono-exponential decay with extracted lifetime of 2.5 ns. With increasing electric field to 15 kV/cm and higher, the decay curve shows a bi-exponential decay with a fast lifetime component of 1.3 ns for 15 kV/cm and 1.1 ns for 50 kV/cm. Kada *et al.* have correlated the mono-exponential-decay and the

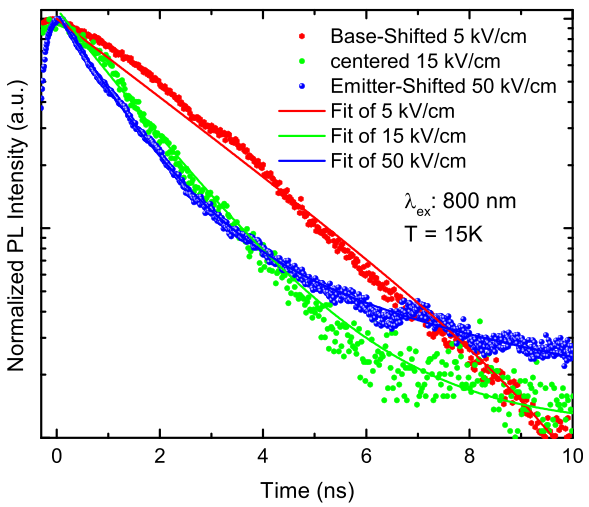


FIG. 5. Electric field dependent ground states PL decay measured at 15 K. The excitation wavelength was 800 nm.

fast component in the bi-exponential decay to the radiative recombination rate in a single QD.[50] The fast component is expected to increase with increasing electric field because the QCSE should reduce wavefunction overlap.[31] However, because an excitation wavelength of 800 nm was chosen (above GaAs band-gap at 15 K), the relaxation of carriers in the GaAs barrier to the ground state is first through the wetting layer and excited states. Due to field introduced broadening,[47] part of the detected ground state PL emission is from the exciton recombination of the tail of the wetting layer and the excited states. Because electrons in excited states or wetting layer states are less bounded, the radiative recombination lifetime is reduced due to increased wavefunction overlap. As a result, the value of fast components in the QD with 50 kV/cm and 15 kV/cm are smaller than the lifetime in the 5 kV/cm QDSC. This reduced fast component as a function of increasing electric field has also been shown by Kasamatsu *et al.* in temperature dependent TRPL measurements using excitation wavelength at 900 nm.[18]

The slow lifetime component is from exciton recombination between different layers along the growth direction. Kojima *et al.* suggested that there is an interconnection between the InAs QDs caused by the elongation of the electron envelope function along the growth direction even with a spacer layer of 40 nm.[34] When the electric field increases from 15 kV/cm to 50 kV/cm, the slow component increases from 2.1 ns to 7.1 ns. This demonstrates that an increasing electric field increases the radiative recombination lifetime by partially separating the electron and hole wavefunctions in the ground state along the growth direction.[10,18]

A half-filled carrier population in the IB is required for TSPA to allow optical transitions of carriers both into and out of the confined states. The IB with partially filled electrons requires reduced radiative recombination and suppressed carrier escape. The higher electric field in the InAs/GaAs QDSC extends the lifetime of radiative recombination but it also enhances the carrier escape. However, TSPA could perhaps still be optimized under an electric field[17] if barrier modifications[51] are made to reduce carrier thermal escape.

The simulations predict that carrier escape is dominated by thermal escape. To experimentally examine the effect of electric field on carrier escape from the ground state, temperature dependent EQE (TDEQE) measurements were also conducted on the investigated QDSCs. Figure 6(a) shows TDEQE normalized to 300 K from the ground state excitation for each design. When the temperature is above 100 K, thermal escape dominates the ground state carrier escape, so the ground state carrier collection in all three samples decreases with lower temperature. When the temperature is decreased below 100 K, the thermal escape rate is reduced below $1 \times 10^7\ s^{-1}$. The TSPA process is also too slow to be considered, given the low-intensity of the monochromatic light. Tunneling in the low electric field QDSCs (5 kV/cm and 15 kV/cm) should be limited since the rate is orders of magnitude less than the radiative recombination rate. One should expect that the EQE of these two QDSCs is near zero below 100 K. However, this was only the case of the 5 kV/cm sample, while the 15 kV/cm showed a residual EQE

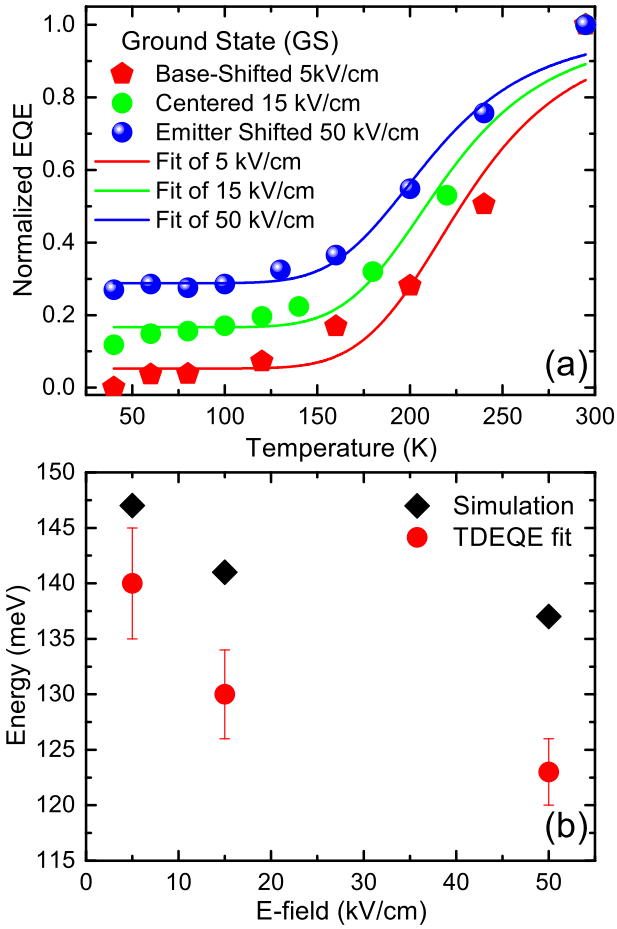


FIG. 6. (a) GS EQE of all three investigated cells; (b) fitted activation energy and calculated effective barrier height of the electrons.

near 15% of its 300 K value. For the QDSC with highest electric field of 50 kV/cm, the simulation in Figure 3(b) shows the tunneling of ground state electron is near $10^7\ s^{-1}$, which is an order of magnitude lower than to the radiative recombination rate ($5 \times 10^8\ s^{-1}$) from TRPL measurements. This would also not account for the high residual EQE (~30% of the 300 K value) observed in the 50 kV/cm sample. There may be two possible reasons for the stable residual EQE observed at temperature below 100 K: (i) carrier collection from the absorption of the tail of the wetting layer and GaAs.[47,52] (ii) A size-selective tunneling effect[53] caused by faster carrier tunneling rate in the smaller dots. Keep in mind that the QD size used in the simulation is only an average value from AFM measurements, while the QDs size is actually a Gaussian distributed around the average value.

To verify the electric field reduced barrier height in the simulation, the temperature dependent EQE can be fit using Equation (5), which is derived from the rate equations for the QDs under steady state conditions.[53] The EQE depends on the fraction of carriers that escape prior to recombining. The numerator of Equation (5) is the total escape rate, which includes thermal escape rate in Equation (1) and tunneling in Equation (2). The denominator refers to the carrier lifetime shown in Equation (3). A radiative recombination lifetime on the order of 1 ns was used for the fitting, and non-radiative recombination was ignored

$$EQE_{normalized} = \frac{\frac{1}{\tau_t} + \frac{1}{\tau_{th}}}{\frac{1}{\tau_{total}}}. \quad (5)$$

Figure 6(b) shows the extracted electric field dependent activation energy using Equation (5) and the barrier height calculated from the band structure simulation. The fit activation energy decreases with increasing electric field, which confirms the theoretical prediction that the effective barrier height decreases with increasing local electric field. The values of the fit activation energy were $140 \pm 5$ meV, $131 \pm 4$ meV, and $123 \pm 3$ meV for the QDSCs with QD local field of 5 kV/cm, 15 kV/cm, and 50 kV/cm, respectively. The values are slightly lower than the effective electron barrier from the band structure simulation, which may be affected by the difference between the size of the QDs in the investigated QDSCs and the QD in the simulation. As well, the difference between the simulation and extracted activation energy increases with increased electric field, which may be because carriers in the 50 kV/cm QDSC experience thermally assisted tunneling[6,8] that was not accounted for the simulation.

Additionally, Figure 7 shows the temperature-dependent EQE normalized to 300 K from the first excited state. In the 50 kV/cm sample, the tunneling escape and thermal escape are almost equivalent at room temperature. Due to the temperature independent fast tunneling in the excited states, only a small reduction (20%) in EQE from 300 K to 60 K is observed in the 50 kV/cm sample. The 15 kV/cm samples shows a similar effect, albeit with a larger drop in EQE with temperature since the tunneling rate in this sample has decreased and is on the same order as the radiative recombination rate. The 5 kV/cm sample shows behavior similar to the ground state, due to limited tunneling from the QD, although some degree of size-dependent tunneling may still result in the observed residual EQE below 75 K. The extracted radiative lifetime from fitting via Equation (4) is on the order of 0.1 ns, which is correlated with the literature value.[54] The extracted activation energy shows the same decreasing trend with increasing electric field. The value of the fit activation energy is $70 \pm 2$ meV, $66 \pm 3$ meV, and $62 \pm 7$ meV for the QDSC with increasing electric field from 5 kV/cm to 50 kV/cm, which is close to the value of the ES barrier height from the band structure simulation.

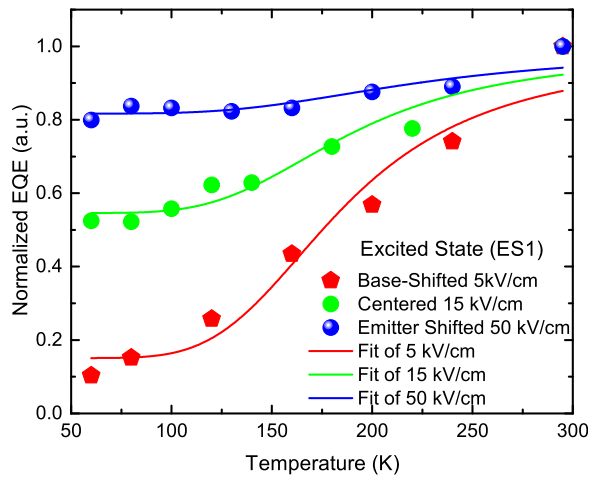


FIG. 7. Temperature dependent normalized first excited state EQE and the fit of the three investigated design with varied electric field around QD.

## IV. CONCLUSION

To achieve a QD-IBSC, TSPA should be the dominant escape process of carriers in the IB. To improve the efficiency of TSPA at room temperature, both carrier escape and recombination in the IB should be suppressed. In the studied InAs/GaAs QDSCs with a varying electric field across the QD embedded region of the device, thermal escape and carrier tunneling are shown as the primary mechanisms of carrier collection at room temperature. Increasing local electric field reduces the effective barrier height by raising the average energy of the electron wave function in the QDs. As a result, both carrier tunneling and thermal escape from InAs/GaAs QDs increase with an increasing electric field. At 300 K, fast thermal escape limits the TSPA in these InAs/GaAs QDSCs. Tunneling escape from excited states becomes dominant only when the electric field exceeds 50 kV/cm. Room temperature EQE shows increased carrier collection from the excited states because of electric field enhanced carriers escape and charge separation. The increased carrier collection from the QD ground state (VB-IB transition) at higher fields may be due to the field introduced broadening of absorption from the wetting layer as well as reduced carrier recapture. On the other hand, the rising slow components with increasing electric field in the low temperature TRPL experiments demonstrate that an increasing electric field extends radiative lifetime by spatially separating electrons and holes. TDEQE measurements show the ground state carrier collection is reduced with decreasing temperature because thermal escape is suppressed, which correlates with the simulations. The simulated effective barrier height was verified by the extracted activation energy from TDEQE. The electric field across InAs/GaAs QDs not only enhances carrier escape from the IB, but also improves charge separation across the intrinsic region that extends carrier radiative lifetime in the IB. To balance the effect of electric field on electron escape and radiative recombination, a proper solar cell design such as wide-band-gap material should be considered to optimize the probability of TSPA.

## ACKNOWLEDGMENTS

This work was supported by the following Grant Nos. NSF DMR-0955752, DOE DE-FG36-08GO18012, NASA SAA3 844, AFRL FA9453-11-C-0253, and the U.S. Government.

[1]A. Luque and A. Martí, Phys. Rev. Lett. **78**, 5014 (1997).
[2]S. Tomić, Phys. Rev. B **82**, 195321 (2010).
[3]Y. Okada, N. J. Ekins-Daukes, T. Kita, R. Tamaki, M. Yoshida, A. Pusch, O. Hess, C. C. Phillips, D. J. Farrell, K. Yoshida, N. Ahsan, Y. Shoji, T. Sogabe, and J.-F. Guillemoles, Appl. Phys. Rev. **2**, 21302 (2015).
[4]K. Driscoll, M. F. Bennett, S. J. Polly, D. V. Forbes, and S. M. Hubbard, Appl. Phys. Lett. **104**, 23119 (2014).

[5]C. G. Bailey, D. V. Forbes, R. P. Raffaelle, and S. M. Hubbard, Appl. Phys. Lett. **98**, 163105 (2011).
[6]E. Antolín, A. Martí, C. D. Farmer, P. G. Linares, E. Hernández, A. M. Sánchez, T. Ben, S. I. Molina, C. R. Stanley, and A. Luque, J. Appl. Phys. **108**, 64513 (2010).
[7]K. A. Sablon, J. W. Little, V. Mitin, A. Sergeev, N. Vagidov, and K. Reinhardt, Nano Lett. **11**, 2311 (2011).
[8]Y. Dai, C. G. Bailey, C. Kerestes, D. V. Forbes, and S. M. Hubbard, in Proceedings of the 38th IEEE Photovoltaic Specialist Conference (PVSC) (2012), pp. 000039–000044.
[9]A. Datas, E. López, I. Ramiro, E. Antolín, A. Martí, A. Luque, R. Tamaki, Y. Shoji, T. Sogabe, and Y. Okada, Phys. Rev. Lett. **114**, 157701 (2015).
[10]A. Creti, V. Tasco, A. Cola, G. Montagna, I. Tarantini, A. Salhi, A. Al-Muhanna, A. Passaseo, and M. Lomascolo, Appl. Phys. Lett. **108**, 63901 (2016).
[11]T. Nozawa, H. Takagi, K. Watanabe, and Y. Arakawa, Nano Lett. **15**, 4483 (2015).
[12]S. Asahi, H. Teranishi, N. Kasamatsu, T. Kada, T. Kaizu, and T. Kita, J. Appl. Phys. **116**, 63510 (2014).
[13]Y. Okada, T. Morioka, K. Yoshida, R. Oshima, Y. Shoji, T. Inoue, and T. Kita, J. Appl. Phys. **109**, 24301 (2011).
[14]D. G. Sellers, S. Polly, S. M. Hubbard, and M. F. Doty, Appl. Phys. Lett. **104**, 223903 (2014).
[15]P. G. Linares, A. Martí, E. Antolín, C. D. Farmer, Í. Ramiro, C. R. Stanley, and A. Luque, Sol. Energy Mater. Sol. Cells **98**, 240 (2012).
[16]I. Ramiro, E. Antolín, A. Martí, C. D. Farmer, C. R. Stanley, and A. Luque, Sol. Energy Mater. Sol. Cells **140**, 299 (2015).
[17]M. Elborg, T. Noda, T. Mano, M. Jo, Y. Sakuma, K. Sakoda, and L. Han, Sol. Energy Mater. Sol. Cells **134**, 108 (2015).
[18]N. Kasamatsu, T. Kada, A. Hasegawa, Y. Harada, and T. Kita, J. Appl. Phys. **115**, 83510 (2014).
[19]S. M. Hubbard, A. Podell, C. Mackos, S. Polly, C. G. Bailey, and D. V. Forbes, Sol. Energy Mater. Sol. Cells **108**, 256 (2013).
[20]C. G. Bailey, D. V. Forbes, S. J. Polly, and Z. S. Bittner, IEEE J. Photovoltaics **2**, 269 (2012).
[21]A. Trellakis, T. Zibold, T. Andlauer, S. Birner, R. K. Smith, R. Morschl, and P. Vogl, J. Comput. Electron. **5**, 285 (2006).
[22]I. Vurgaftman, J. R. Meyer, and L. R. Ram-Mohan, J. Appl. Phys. **89**, 5815 (2001).
[23]S.-S. Li and J.-B. Xia, J. Appl. Phys. **88**, 7171 (2000).
[24]S. Hellstroem and S. M. Hubbard, in Proceedings of the IEEE 40th Photovoltaic Specialist Conference (PVSC) (2014), pp. 1037–1040.
[25]H. Schneider and K. V. Klitzing, Phys. Rev. B **38**, 6160 (1988).
[26]A. Larsson, P. A. Andrekson, S. T. Eng, and A. Yariv, IEEE J. Quantum Electron. **24**, 787 (1988).
[27]A. M. Fox, D. A. B. Miller, G. Livescu, J. E. Cunningham, and W. Y. Jan, IEEE J. Quantum Electron. **27**, 2281 (1991).
[28]A. Alemu and A. Freundlich, IEEE J. Photovoltaics **2**, 256 (2012).
[29]A. P. Zhou and W. D. Sheng, Eur. Phys. J. B **68**, 233 (2009).
[30]D. Bimberg, M. Grundmann, and N. N. Ledentsov, *Quantum Dot Heterostructures* (John Wiley, Chichester, [Eng.], New York, 1999).
[31]T. Miyazawa, T. Nakaoka, T. Usuki, J. Tatebayashi, Y. Arakawa, S. Hirose, K. Takemoto, M. Takatsu, and N. Yokoyama, J. Appl. Phys. **104**, 13504 (2008).
[32]M. Paillard, X. Marie, E. Vanelle, T. Amand, V. K. Kalevich, A. R. Kovsh, A. E. Zhukov, and V. M. Ustinov, Appl. Phys. Lett. **76**, 76 (2000).
[33]X. L. Zhou, Y. H. Chen, H. Y. Zhang, and G. Y. Zhou, J. Appl. Phys. **109**, 83501 (2011).
[34]O. Kojima, H. Nakatani, T. Kita, O. Wada, K. Akahane, and M. Tsuchiya, J. Appl. Phys. **103**, 113504 (2008).
[35]R. Heitz, M. Grundmann, N. N. Ledentsov, L. Eckey, M. Veit, D. Bimberg, V. M. Ustinov, A. Y. Egorov, A. E. Zhukov, P. S. Kop'ev, and Z. I. Alferov, Appl. Phys. Lett. **68**, 361 (1996).
[36]E. Harbord, P. Spencer, E. Clarke, and R. Murray, Phys. Rev. B **80**, 195312 (2009).
[37]V. Aroutiounian, S. Petrosyan, and A. Khachatryan, Sol. Energy Mater. Sol. Cells **89**, 165 (2005).
[38]J. Hwang, A. J. Martin, J. M. Millunchick, and J. D. Phillips, J. Appl. Phys. **111**, 74514 (2012).
[39]S. J. Polly, Ph.D. thesis (2015).
[40]D. V. Forbes, A. M. Podell, M. A. Slocum, S. J. Polly, and S. M. Hubbard, Mater. Sci. Semicond. Process. **16**, 1148 (2013).
[41]D. V. Forbes, Y. Dai, S. J. Polly, S. Hellstroem, C. Bailey, and S. M. Hubbard, in Proceedings of the IEEE 40th Photovoltaic Specialist Conference (PVSC) (2014), pp. 3488–3491.
[42]R. Jakomin, R. M. S. Kawabata, R. T. Mourão, D. N. Micha, M. P. Pires, H. Xie, A. M. Fischer, F. A. Ponce, and P. L. Souza, J. Appl. Phys. **116**, 93511 (2014).
[43]H. Xie, R. Prioli, A. M. Fischer, F. A. Ponce, R. M. S. Kawabata, L. D. Pinto, R. Jakomin, M. P. Pires, and P. L. Souza, J. Appl. Phys. **120**, 34301 (2016).
[44]A. Martí, L. Cuadra, and A. Luque, Physica E **14**, 150 (2002).
[45]D. B. Malins, A. Gomez-Iglesias, P. Spencer, E. Clarke, R. Murray, and A. Miller, Electron. Lett. **43**, 686 (2007).
[46]R. Prasanth, J. Appl. Phys. **99**, 54501 (2006).
[47]P. W. Fry, I. E. Itskevich, S. R. Parnell, J. J. Finley, L. R. Wilson, K. L. Schumacher, D. J. Mowbray, M. S. Skolnick, M. Al-Khafaji, A. G. Cullis, M. Hopkinson, J. C. Clark, and G. Hill, Phys. Rev. B **62**, 16784 (2000).
[48]M. Gioannini, A. P. Cedola, N. Di Santo, F. Bertazzi, and F. Cappelluti, IEEE J. Photovoltaics **3**, 1271 (2013).
[49]L. M. Kong, Z. C. Feng, Z. Y. Wu, and W. Lu, Semicond. Sci. Technol. **23**, 75044 (2008).
[50]T. Kada, S. Asahi, T. Kaizu, Y. Harada, T. Kita, R. Tamaki, Y. Okada, and K. Miyano, Phys. Rev. B **91**, 201303 (2015).
[51]Y. Dai, M. A. Slocum, Z. Bittner, S. Hellstroem, D. V. Forbes, and S. M. Hubbard, in Proceddings of the IEEE 43rd Photovoltaic Specialist Conference (PVSC) (2016), pp. 0151–0154.
[52]T. Li, R. E. Bartolo, and M. Dagenais, Appl. Phys. Lett. **103**, 141113 (2013).
[53]W.-H. Chang, T. M. Hsu, C. C. Huang, S. L. Hsu, C. Y. Lai, N. T. Yeh, T. E. Nee, and J.-I. Chyi, Phys. Rev. B **62**, 6959 (2000).
[54]E. Harbord, S. Iwamoto, Y. Arakawa, P. Spencer, E. Clarke, and R. Murray, Appl. Phys. Lett. **101**, 183108 (2012).